

## The Black Hole–Bulge Relationship in QSOs

Gregory A. Shields<sup>1</sup>, Karl Gebhardt<sup>1</sup>, Sarah Salviander<sup>1</sup>, Beverley J. Wills<sup>1</sup>, Bingrong Xie<sup>2</sup>,  
Michael S. Brotherton<sup>3</sup>, Juntao Yuan<sup>1</sup>, and Matthias Dietrich<sup>4</sup>

### ABSTRACT

We use QSO emission-line widths to examine the  $M_{BH} - \sigma_*$  relationship as a function of redshift and to extend the relationship to larger masses. Supermassive black holes in galactic nuclei are closely related to the bulge of the host galaxy. The mass of the black hole,  $M_{BH}$ , increases with the bulge luminosity and with the velocity dispersion of the bulge stars,  $\sigma_*$ . An important clue to the origin of this correlation would be an observational determination of the evolution, if any, in the  $M_{BH} - \sigma_*$  relationship as a function of cosmic time. The high luminosity of QSOs affords the potential for studies at large redshifts. We derive black hole masses from the continuum luminosity and the width of the broad H $\beta$  line and  $\sigma_*$  from the width of the narrow [O III] lines. We find that radio quiet QSOs conform to the established  $M_{BH} - \sigma_*$  relationship up to values  $M_{BH} \approx 10^{10} M_\odot$ , with no discernible change in the relationship out to redshifts of  $z \approx 3$ . These results are consistent with the idea that the growth of supermassive black holes and massive bulges occurred simultaneously.

*Subject headings:* galaxies: active — quasars: general — black hole physics

---

<sup>1</sup>Department of Astronomy, University of Texas, Austin, TX 78712; shields@astro.as.utexas.edu, gebhardt@astro.as.utexas.edu, triples@astro.as.utexas.edu, bev@astro.as.utexas.edu, juntao@astro.as.utexas.edu

<sup>2</sup>Department of Physics and Astronomy, Rutgers, The State University of New Jersey, P.O. Box 849, Piscataway, NJ 08855-0849; xiebr@physics.rutgers.edu

<sup>3</sup>National Optical Astronomy Observatories, 950 N. Cherry Ave., Tucson, AZ 85726; mbrother@ohmah.tuc.noao.edu

<sup>4</sup>Department of Astronomy, University of Florida, 211 Bryant Space Science Center, Gainesville, FL 32611-2055; dietrich@astro.ufl.edu

## 1. INTRODUCTION

The evolution of supermassive black holes and that of their host galaxies appear to be closely coupled. Every bulge system studied with high spatial resolution shows a central black hole, presumably a relic of AGN activity (Kormendy & Richstone 1995; Richstone et al. 1999; Kormendy & Gebhardt 2001). The black hole mass is roughly proportional to the luminosity of the bulge of the host galaxy, albeit with scatter of  $\sim 0.5$  dex in  $M_{BH}$  (Magorrian et al. 1998). Gebhardt et al. (2000a) and Ferrarese & Merritt (2000) found a tighter correlation involving  $M_{BH}$  and  $\sigma_*$ , where  $\sigma_*$  is the stellar line-of-sight velocity dispersion at radii outside the gravitational influence of the black hole. Tremaine et al. (2002) give this relationship as

$$M_{BH} = (10^{8.13} M_{\odot})(\sigma_*/200 \text{ km s}^{-1})^{4.02}. \quad (1)$$

with an intrinsic scatter  $\leq 30\%$ . (The measure of scatter here is  $1 \sigma$  for  $M_{BH}$  at fixed bulge luminosity or  $\sigma_*$ , respectively.) Theoretical interpretations of this correlation (e.g., Silk & Rees 1998; Adams et al. 2001; Burkert & Silk 2001; Ostriker 2001; Balberg & Shapiro 2002; Haehnelt & Kauffmann 2000) variously would have the black hole form before, during, or after bulge formation. Given this uncertainty, measurements of  $M_{BH}$  in galaxies with large look-back times would be valuable. Most promising would be a measurement of the  $M_{BH} - \sigma_*$  relationship at high redshift, because the relatively small scatter of this relationship in the local universe should make it possible to discern even modest changes over time.

Unfortunately, measurements of  $M_{BH}$  and  $\sigma_*$  at high redshift are challenging because spatially resolved kinematical studies are feasible only for nearby systems. However, recent work indicates that useful measures of  $M_{BH}$  in AGN are possible (see Peterson 1997; Wandel, Peterson, & Malkan 1999). McLure & Dunlop (2001) and Wandel (2001) summarize the “reverberation” and “photoionization” methods to measure  $M_{BH}$  in Seyfert galaxies. The results correlate with bulge luminosity in a way consistent with nearby galaxies, confirming the calibration of  $M_{BH}$  for AGN. However, the host galaxy brightness is difficult to measure in the presence of a bright active nucleus, and a direct measurement of  $\sigma_*$  for quasar host galaxies using stellar absorption-lines is likewise difficult. Alternatively, the narrow emission-line widths can serve as a surrogate for  $\sigma_*$ . Nelson & Whittle (1996) find agreement between narrow emission-line widths in AGNs and widths measured from stellar absorption-line kinematics. On this basis, Nelson (2000) proposes to use the width of the [OIII]  $\lambda\lambda 5007, 4959$  lines of AGN as a surrogate for  $\sigma_*$ . Thus, one takes  $\sigma_* \approx \sigma_{[O III]}$ , where  $\sigma_{[O III]} \equiv \text{FWHM}([O III])/2.35$  and FWHM is the full width at half maximum. The divisor 2.35 relates  $\sigma$  and FWHM for a Gaussian profile. Taking black hole masses from reverberation mapping, Nelson finds no systematic offset in the  $M_{BH} - \sigma_{[O III]}$  relationship between

low redshift AGN measured this way and measurements of galaxies based on observed stellar velocity dispersions.

In this paper, we use emission-line widths to study the  $M_{BH} - \sigma_{[O III]}$  relationship for a sample of quasars at redshifts up to 3.3. Our goal is to assess the evolutionary history of black hole growth compared with that of the host galaxy. In Section 2, we describe the derivation of  $M_{BH}$  and the use of the [O III] line width as a surrogate for  $\sigma_*$ . Then we describe our adopted data set, which relies on published data covering a range of redshift together with our unpublished observations of low redshift QSOs. In Section 3, we present the results, and we examine the trend of  $M_{BH}$  with  $\sigma_{[O III]}$  and the redshift dependence of this relationship. In Section 4, we discuss these results and the needed improvements. Throughout our discussion, we use a cosmology with  $H_0 = 70 \text{ km s}^{-1} \text{ Mpc}^{-1}$ ,  $\Omega_M = 0.3$ ,  $\Omega_\Lambda = 0.7$ . All values of luminosity used in this paper are corrected to our adopted cosmological parameters.

## 2. METHOD

### 2.1. Calculation of Black Hole Masses

The derivation of black hole masses from AGN broad line widths has been discussed by a number of authors, recently including Laor (1998), Wandel et al. (1999), Kaspi et al. (2000), Vestergaard (2002), and McLure & Dunlop (2001). The method relies on assuming that the line widths, at least for some lines, are dominated by orbital motion of the emitting gas in the gravitation potential of the black hole. This is supported by the generally symmetrical time variability of the wings, and the decrease in line width with increasing radius for different lines in a given object (see Wandel et al. 1999, and references therein). The black hole mass is then given by  $M_{BH} = v^2 R / G$ , where  $v$  and  $R$  are an appropriate velocity and radius for the BLR. Deriving  $v$  and  $R$  from the observations is not entirely straightforward, as the emitting gas spans a range of radii and velocities. Pragmatically, the radius is derived from “reverberation mapping” or “echo mapping” studies that monitor the variation of the continuum and emission lines. The characteristic time lag between continuum variations and the response of a given line gives a measure of the radius of the region emitting that line (see review by Peterson 1993). Given this determination of  $R$ , one needs a measure of line width which, combined with this radius, gives the correct black hole mass. This choice can be parameterized as  $v = f \times \text{FWHM}$  for the line. Some authors use  $f = \sqrt{3}/2$ , appropriate for isotropic velocities. However, McLure & Dunlop (2001) argue that allowance for a flattened geometry of the BLR is preferable. Most work has employed the Balmer lines, in particular  $H\beta$ . Black hole masses determined in this way for AGN with measured  $\sigma_*$  show overall agreement with the  $M_{BH} - \sigma_*$  relationship (Gebhardt et al. 2000b; Ferrarese et al. 2001;

McLure & Dunlop 2001).

The work of Wandel et al. (1999) and Kaspi et al. (2000) generated a set of BLR radii based on variability of the Balmer lines for 17 Seyfert 1 (Sy 1) galaxies and 17 PG QSOs. This work supports earlier indications that the BLR radius increases with luminosity, approximately as  $R \propto L^{0.5}$ . Photoionization physics suggests  $R \propto L^{0.5}$ , and this is also consistent with the idea that the BLR radius may be limited by the minimum radius at which dust grains survive (Netzer & Laor 1993). This relationship is enormously useful, for it opens the door to measuring black hole masses in large numbers of AGN from measurements of line width and luminosity at a single epoch. By determining the BLR radius in this way, one avoids the need for long series of observations of variability, which are in any case impractical for luminous, high redshift QSOs with long variability timescales. The use of such “photoionization masses”, calibrated in terms of echo results, has been discussed by several authors, including Wandel et al. (1999) and Vestergaard (2002). There is some controversy over the slope of the radius-luminosity relationship. Kaspi et al. (2000) find  $R \propto L^{0.7}$ , based on echo radii. However, McLure & Jarvis (2002; see also Maoz 2002), find  $R \propto L^{0.61}$ . On this basis, they fit the echo masses with  $M_{BH} = (10^{7.63} M_{\odot}) v_{3000}^2 L_{44}^{0.61}$ , where  $v_{3000} \equiv FWHM(H\beta)/3000 \text{ km s}^{-1}$  and  $L_{44} \equiv \lambda L_{\lambda}(5100 \text{ \AA})/(10^{44} \text{ erg s}^{-1})$ , using the same cosmology that we have adopted. The difference in slope results from several factors, including a new echo mass for NGC 4051, different continuum luminosities, and the cosmological model. Here we take for our primary calibration the physically motivated slope  $R \propto L^{0.5}$ . We adopt the  $L^{0.5}$  fit shown in Figure 6 of Kaspi et al.,

$$M_{BH} = (10^{7.69} M_{\odot}) v_{3000}^2 L_{44}^{0.5}, \quad (2)$$

where we have adjusted the coefficient to our cosmology. (This expression agrees with our own fitting of the Kaspi et al data and depends little on NGC 4051 because the slope is fixed.)

We use the  $H\beta$  line width in this fashion to determine  $M_{BH}$ , adopting the calibration of equation (2) for most of our discussion but illustrating the key results also for  $M_{BH} \propto L^{0.61}$ . McLure & Jarvis and Vestergaard (2002) discuss the use of other lines. The use of the  $\lambda 5100$  continuum follows Wandel et al. (1999) and Kaspi et al. (2000). McLure & Jarvis (2002) and Laor et al. (1997) argue that the  $\lambda 3000 \text{ \AA}$  continuum may work better, but the differences are not great. The  $\lambda 5100$  continuum has the practical advantage that it can be measured in the same spectra as the  $H\beta$  and [O III] lines, and it is less affected by dust extinction.

## 2.2. [O III] Lines in AGN

Nelson & Whittle (1996) have compared [O III] line widths and stellar velocity dispersions in AGN, finding generally good agreement. For the quantity  $\log \sigma_{[\text{O III}]} / \sigma_*$ , they find a mean  $0.00 \pm 0.01$  and a dispersion  $\sigma = 0.20$ , supporting the idea that the motions of the NLR gas are largely determined by the gravitational potential of the host galaxy. This is reinforced by the analysis by Nelson (2000), who shows essentially that  $\sigma_{[\text{O III}]}$  and  $M_{BH}$  obey equation (1) for AGN with echo values of  $M_{BH}$ . These results support the use of  $\sigma_{[\text{O III}]}$  as a surrogate for  $\sigma_*$ . A caution, however, is that [O III] profiles often have substantial asymmetry and non-Gaussian profiles, possibly resulting from outflow combined with extinction of the far side of the NLR (e.g., Wilson & Heckman 1985; Nelson & Whittle 1995).

Radio loud AGN tend to have stronger [O III] emission than radio quiet objects, as reflected in “Eigenvector 1” of Boroson & Green (1992). Radio jets may contribute to the motions of the NLR gas (Nelson & Whittle 1996). For this reason, we emphasize radio quiet objects in this paper, and we discuss radio loud objects separately.

## 2.3. New Observations

We include here results from an unpublished set of spectra of QSOs obtained at McDonald Observatory with the Large Cassegrain Spectrograph (LCS) on the 2.7-meter telescope. These objects correspond to the X-ray sample studied by Laor et al. (1997), which is in turn taken from the Bright Quasar Survey based on the Palomar Green (PG) survey (Boroson & Green 1992; Schmidt & Green 1983). We take values of FWHM( $\text{H}\beta$ ) from Boroson & Green. The instrumental resolution was 150 to 180  $\text{km s}^{-1}$  FWHM, depending on redshift. Emission from Fe II blends was removed from the spectra with the aid of the Boroson & Green (1992) template. Table 1 gives the [O III] widths for 2 RL and 14 RQ objects in the redshift range 0.09 to 0.33 derived from our spectra. We use here the results of directly measuring the half-maximum point of the observed line profile rather than by fitting any kind of curve. The width of  $\lambda 4959$  was noted for corroboration. (See below for a discussion of methods of measuring the [O III] line width.) Our own measurements of FWHM for  $\text{H}\beta$  ranged from 0.95 to 1.35 times the BG92 values, with a mean ratio of 1.09. This may give some indication of systematic uncertainties arising from Fe II subtraction and fitting procedure, although real temporal variations may affect individual objects. For our PG sample, continuum luminosities were taken from Laor et al. (1997). Table 2 lists the redshift, adopted line widths, continuum luminosity, and black hole mass derived from equation (2).

## 2.4. Data from the literature

We have drawn observations of  $H\beta$  and [O III] from several published sources. These are listed below, roughly in order of decreasing redshift. The results are given in Table 2. The quoted line widths are intrinsic values after subtraction of the instrumental width.

(1) Dietrich et al. (2002, “D02”) present infrared spectra for six QSOs with  $z \approx 3.4$ , placing  $H\beta$  and [O III] in the infrared  $K$ -band wavelength region. Of these, Q0256-0000 and Q0302-0019 have [O III] lines of adequate strength to measure the line width. We have measured the FWHM of [O III] and  $H\beta$  from the original data, using a direct measurement of the FWHM. We subtract in quadrature the instrumental width of  $400 \text{ km s}^{-1}$ . We find  $\text{FWHM}([\text{O III}]) = 838 \pm 29 \text{ km s}^{-1}$  for Q0256-0000 and  $743 \pm 19 \text{ km s}^{-1}$  for Q0302-0019, where the quoted errors reflect only the noise in the data. (For a single Gaussian fit to the [O III] profiles, we find  $886$  and  $846 \text{ km s}^{-1}$ , respectively. These are  $0.02$ ,  $0.05$  dex larger than the direct measurements. The sense of the difference is typical, but the magnitude is not significant for our purposes. The appropriateness of Gaussian profiles is discussed below.) We corrected for the narrow component of  $H\beta$  by assuming a typical ratio of  $\lambda 5007$  to narrow  $H\beta$  of  $10$  to  $1$ , as discussed in Brotherton (1996b, “B96b”) and references therein. The quoted noise errors and the likely error resulting from subtraction of the narrow  $H\beta$  component are small compared to scatter among objects described below. Continuum luminosities are discussed below.

(2) McIntosh et al. (1999, “M99”) give  $H$ -band spectra of  $32$  luminous QSOs at  $2.0 \leq z \leq 2.5$ , covering  $H\beta$  and [O III]. The instrumental resolution is about  $500 \text{ km s}^{-1}$ . The signal-to-noise ratio (S/N) of the spectra is poor in some cases. Therefore, we present in Figures 1 and 2 two different data selections. For the “full” sample, we include all objects for which M99 give FWHM for both  $H\beta$  and [O III]. For the “select” sample, we include those QSOs for which the greatest of the positive and negative errors in FWHM for both  $H\beta$  and [O III], as a fraction of FWHM, is  $0.33$  or less. This results in a list of  $4$  radio loud (RL) and  $4$  radio quiet (RQ) objects. The “full” sample offers a larger number of objects for averaging purposes, and it avoids the question of bias in selecting the better measurements. However, it contains some rather uncertain measurements and may exaggerate the true dispersion of the data. The “select” sample is consistent with a reasonable judgment of the most reliable measurements, based on the S/N of the spectra. (The spectra are given in M99.) M99 quote a FWHM for the “total  $H\beta$ ” profile and for the “broad  $H\beta$ ” component. The “broad  $H\beta$ ” width exceeds the “total” width by more than can be accounted for by the removal of a narrow  $H\beta$  component with a typical intensity ratio to [O III] (see above). We have carried out our own fits to the M99 data for some representative objects, including a broad  $H\beta$  component plus a narrow  $H\beta$  component with the same width as the [O III] lines. We find

that the width of the broad  $H\beta$  component is fairly close to M99’s “total  $H\beta$ ” width and much narrower than their quoted “broad  $H\beta$ ” width. Accordingly, we use FWHM for  $\lambda 5007$  and  $H\beta_{total}$  from Table 4 of M99 and a RL/RQ type from their Table 2. See Vestergaard (2002) for a discussion of the appropriate measure of  $H\beta$  width for determinations of black hole mass. Average errors in  $FWHM([O III])$  are  $\pm 0.12, 0.16$  dex for the RL, RQ objects in the “full” sample and  $0.07, 0.10$  dex for the “select” sample, respectively. Errors are in most cases smaller for  $H\beta$  than  $[O III]$  width. Error bars are omitted from our figures for clarity, and the reader should bear these errors in mind.

(3) Brotherton (1996a, “B96a”) gives results of infrared spectroscopy of 18 RL and 14 RQ QSOs ranging in redshift from 0.7 to 2.5. Of these, 11 RQ and 7 RL objects were observed with the Cryogenic Spectrometer (CRSP) on the 2.1 meter telescope at Kitt Peak National Observatory (KPNO). The remaining objects were observed with other setups giving inadequate spectral resolution, or are included in B96b. All our data sources give line widths corrected for instrumental resolution except B96a. For B96a, we subtract in quadrature the instrumental resolution of 470, 600, and 460  $\text{km s}^{-1}$  for I, J, and H band observations, respectively, as estimated by Brotherton (2002). Our “full” data set includes all 11 CRSP radio quiet objects. For the “select” sample, we use all objects for which the fractional error in  $FWHM([O III])$  is  $\leq 0.10$  (Brotherton 2002). This is based on the error in the corrected line widths resulting from the formal error in the original Gaussian fits by B96a. These errors are not directly comparable with those of M99, which involve template fitting and a Monte Carlo error analysis. However, the chosen cutoff agrees with a reasonable judgment of the most reliable measurements, based on the S/N of the spectra. Among the radio quiet objects, the selected ones comprise four of the six CRSP objects for which B96a gives a quality flag of “A”. The select RL sample consists of 4 of the 5 CRSP “A” objects. (The fifth is PKS 0424-131, which is also in the M99 select sample. We include the B96a measurement in Table 2 for comparison.) The  $[O III]$  widths tabulated by B96a involve single Gaussian fits. From the spectra, we have estimated  $FWHM([O III])$  by direct measurement and find typical agreement within about 10% with the adopted Gaussian fits for the RL and RQ select objects. B96a also made no correction for the NLR contribution to the  $H\beta$  profile. None of the spectra shows a prominent narrow line component of  $H\beta$ . For a typical ratio of  $\lambda 5007$  to narrow  $H\beta$  of 10 to 1, the correction would on average increase  $FWHM(H\beta)$  by 11% for the RL select objects and 7% for the RQ select objects. These differences are not significant for our purposes. In addition to FWHM for  $H\beta$  and  $[O III]$  we took from Chapter 6 of B96a the apparent  $V$  magnitudes and RL/RQ classifications of the subject QSOs. We note that 1120+01 is a lens candidate, although it may be a true binary QSO (Kochanek 2002). Michalitsianos et al. (1997) suggest that the amplification factor could be as large as 100. Correction for lensing would lower  $M_{BH}$  as  $L^{0.5}$  from the

value in Table 2 and Figure 1. Perhaps the  $M_{BH} - \sigma_{[O III]}$  relation has potential as an indicator of lensing.

(4) B96b studied profiles of  $H\beta$  and  $[O III]$  in 60 radio loud quasars with  $0.05 \leq z \leq 0.93$ . The instrumental resolution was 150 to 300  $\text{km s}^{-1}$ . We used the FWHM for  $H\beta$  and  $[O III]$  from his Tables 3 and 4. Brotherton gives a quality flag A or B for 37 objects. We judged 6 of these to be unsuitable by visual inspection of the spectra, typically because the broad  $H\beta$  line was weak or had an unusual profile. (The spectra are given in in B96b.) We also eliminated those objects for which we could not obtain a flux density at 5100  $\text{\AA}$  rest wavelength from available spectra, as described below. This left a sample of 23 QSOs that are included in Table 2.

(5) Grupe et al. (1999, “G99”) discuss optical emission-line properties of 76 bright soft X-ray selected AGN, based on spectra with a resolution of  $\sim 5 \text{\AA}$  FWHM ( $\sim 300 \text{ km s}^{-1}$ ). Redshifts and line widths are taken from Table 1 of G99. The  $[O III]$  line width was measured using a single Gaussian fit. We selected the 33 objects for which the fractional uncertainty in FWHM was better than 0.10 both for  $H\beta$  and  $[O III]$ . Four of these were eliminated as unsuitable on the basis of inspection of the spectra as reproduced in Grupe (1996), and one for radio confusion. Two of the remaining objects were found from NED <sup>5</sup> to be radio loud, leaving a sample of 26 radio quiet objects.

## 2.5. Continuum Luminosity

The luminosities for our samples come from heterogeneous sources. An assumed power law  $F_\nu \propto \nu^{-0.5}$  was used when necessary to scale the measurements to 5100  $\text{\AA}$  rest wavelength. Magnitudes were converted to flux densities  $F_\nu$  as prescribed by Allen (1973). When absolute magnitudes or specific luminosities were given, these were adjusted to our adopted cosmology.

For D02, the continuum flux density at 5100  $\text{\AA}$  rest wavelength was measured from the published spectra. For M99 we used  $L_\nu(V)$  from their Table 2, and for B96a we used the apparent V magnitude given in his Chapter 6. For B96b we used flux densities taken from spectrophotometry described by Netzer et al. (1995) and Wills et al. (1995) and unpublished spectrophotometry (Wills and Brotherton 2002) when available and otherwise took them from Figure 1 of B96b. Objects were omitted when neither of these was available, or when the result differed by more than 0.5 dex from the flux density at 5100  $\text{\AA}$  estimated

---

<sup>5</sup>The NASA/IPAC Extragalactic Database (NED) is operated by the Jet Propulsion Laboratory, California Institute of Technology, under contract with the National Aeronautics and Space Administration.



from the absolute visual magnitude  $M_{abs}$  quoted by B96b (taken from Véron-Cetty & Véron 1989). For G99, we measured the optical continuum flux density from the published spectra.

We have not attempted a correction for a contribution to the continuum from the host galaxy. This is unlikely to have a large effect on our conclusions, because  $M_{BH}$  scales only as  $L_\nu^{1/2}$ . We have estimated the host galaxy luminosity from the value of  $\sigma_{[O III]}$  for our individual AGN, using the Faber-Jackson relation (Forbes & Ponman 1999; Bernardi et al. 2001),  $M_V = -20.57 - 2.5 [4 \log(\sigma_{[O III]}/220 \text{ km s}^{-1})]$ . For the adopted RL and RQ objects in the D02, M99, B96, B96b, and PG samples, the average value of  $L_{bulge}/L_{observed}$  is only 2 or 3 percent, and 7 percent for G99. Thus, we have assumed that the measured flux is dominated by the AGN continuum for the adopted spectra of all objects.

## 2.6. Radio Loudness

Objects in the sample were divided into radio-quiet and radio-loud using the radio-to-optical ratio,  $R_{ro} = F_\nu(5 \text{ GHz})/F_\nu(4400\text{\AA})$  as defined by Kellermann et al. (1989), where  $R_{ro} > 10$  designates a radio-loud QSO. For our PG sample, we used values for  $R_{ro}$  from Boroson & Green (1992); for B96a we used values from that reference; for D02 we used values from Hooper et al. (1995); and for M99 we used values from that paper.

For G99 we obtained flux densities at 5 GHz, 4.85 GHz, or 1.4 GHz from photometric points in NED; otherwise, we measured the flux density from NRAO VLA Sky Survey (NVSS) radio flux density maps at 1.4 GHz (Condon et al. 1998). We assumed unresolved single, or very occasionally, double unresolved components. The angular resolution of NVSS of  $45''$  (Condon et al. 1998) includes the extended structure for nearly all QSOs. When no detection was listed or evident on the maps, we assumed that the object was radio quiet. For radio flux densities at frequencies other than 5 GHz we extrapolate to  $F_\nu(5 \text{ GHz})$  assuming  $F_\nu \propto \nu^{-0.7}$ . Subtleties in the definition of  $R_{ro}$  and continuum slope have little effect for our purposes, because of wide range in  $R_{ro}$  values between RQ and RL objects. For purposes of computing  $R_{ro}$ , optical continuum flux densities were found as described above, or taken from NED, and corrected to rest wavelength  $\lambda 4400$  using  $L_\nu \propto \nu^{-0.5}$ .

### 3. RESULTS

#### 3.1. The $M_{BH} - \sigma_{[O III]}$ relationship

Figures 1 and 2 show results for the RQ objects, based on equation (2). Figure 1 includes results for the full samples described above for the M99 and B96a data sets, and Figure 2 shows the select samples. (The data for the other sources is the same.) On average, the QSO results show good agreement with equation (1), shown as the straight line in Figures 1 and 2. This agreement supports the use of photoionization masses for  $M_{BH}$  and the use of the [O III] line width as a surrogate for  $\sigma_*$  to masses over  $10^9 M_\odot$ . However, we emphasize that the close alignment of the massive, high redshift objects in the upper right part of Figure 2 is better than expected from the errors (see discussion above) and must be to some degree fortuitous. The scatter in the PG sample may give a better indication of the scatter resulting from measurement errors together with true variations among objects, as discussed below. We assign significance only to the average agreement of the high redshift points as a group with the  $M_{BH} - \sigma_*$  trend.

We also show in Figures 1 and 2 the objects listed in Table 1 of Nelson (2000). The Nelson points agree in the mean with our results but show less scatter around the Tremaine et al. (2002) line. The echo masses used by Nelson are presumably more accurate than the photoionization masses used here. Also, Nelson restricted his study to data with spectral resolution  $R > 1500$ . (Included in the Nelson points in Figures 1 and 2 are two objects in common with our PG sample, namely 0953+414 and 1411+442.)

If the high redshift and Nelson (2000) points are removed from Figure 1, the scatter in the remaining points is too large to define accurately the slope of the  $M_{BH} - \sigma_{[O III]}$  trend. However, our philosophy here is that the  $M_{BH} - \sigma_*$  relationship is well established, and we are interested in examining the agreement of the AGN data with that relationship. The lower redshift points agree in the mean with equation 1, and this supports our working hypothesis that photoionization masses and  $\sigma_{[O III]}$  can be used as a substitute for direct measurements of  $M_{BH}$  and  $\sigma_*$  in AGN. This is the basis for our discussion of the redshift dependence below.

Nelson & Whittle (1996) found that AGN with powerful, linear radio sources sometimes have  $FWHM([O III])$  larger than expected for the value of  $\sigma_*$ . Figure 3 shows the radio loud objects from our data set, using the select sample for B96a and M99. Objects from most of the data sets scatter around equation (1). However, the measurements of B96b generally stand above and to the left of the trend. One issue may be the procedure for measuring the FWHM of [O III]. Some workers fit a Gaussian and quote the FWHM of this fit. B96b instead gives a direct measurement of the width at the half-maximum level of the

observed line profile, which is feasible only when the data have good spectral resolution and signal-to-noise ratio. For four objects in common between the single Gaussian fit of B96a and the direct measurement of B96b, the B96b width on average is narrower by  $\sim 0.2$  dex. A single Gaussian fit may be affected by broad wings or asymmetry of the line profile and by a tendency to smooth the line peak. This may explain some of the displacement of the B96b points in Figure 2. On the other hand, we also made a direct measurement of  $FWHM([O III])$  for our PG sample, and in Figures 1 and 2 our results do not share the displacement of the B96b sample. Consistent with this, we find that Gaussian fits to [O III] for our PG sample are only 0.04 dex wider on average than the direct measurements used here. As a further illustration, we measured  $FWHM([O III])$  using a Gaussian fit for many of the M99 objects, using the original data. The Gaussian widths are always wider than the M99 values, which should approximate a direct measurement because of the multiple template fit used by M99. For 3 RQ objects in our select sample for M99, the Gaussians are wider by an average of 0.08 dex. However, a few objects, typically with weak or strongly asymmetrical [O III], show differences in FWHM approaching a factor 2. Accurate results using [O III] as a surrogate for  $\sigma_*$  will require careful attention to the shape of the line profile.

### 3.2. Redshift Dependence

The  $M_{BH} - \sigma_{[O III]}$  relationship shown in Figures 1 and 2 provides a basis for assessing the evolution of the relationship with redshift. The B96a, D02, and M99 objects fall in the redshift range 1 to 3.3. These objects do not systematically depart from the overall  $M_{BH} - \sigma_{[O III]}$  relationship. In order to display the trend as a function of redshift, we use a fictitious “[O III] mass”  $M_{[O III]}$  defined as the mass given by equation (1) with  $\sigma_{[O III]}$  in place of  $\sigma_*$ . The quantity  $\Delta \log M \equiv \log M_{BH} - \log M_{[O III]}$  is then a measure of the vertical deviation of a given object from the Tremaine et al. (2002) mean trend in Figures 1 - 3. In Figures 4 and 5, we plot this quantity as a function of redshift for our full and select RQ samples, respectively. In the mean, the high redshift objects show little deviation from the  $M_{BH} - \sigma_*$  trend. Because the most massive objects are the high redshift objects, we cannot independently assess the slope of the  $M_{BH} - \sigma_{[O III]}$  relationship and the redshift dependence. Our point is that *the data are consistent with a  $M_{BH} - \sigma_{[O III]}$  relationship that extends to high masses with a slope close to that of Tremaine et al. (2002) and that does not evolve strongly with time.*

A quantitative measure of the adherence of the high redshift objects to the low redshift trend is difficult, given the small number of high redshift objects in the select sample and the various systematic errors. We may estimate the intrinsic scatter of the high redshift samples

on the basis of the PG sample, which has the higher luminosity of the low redshift samples. The RQ objects in our PG sample show a mean  $\Delta \log M$  of +0.10 and a dispersion 0.5 ( $1 \sigma$ ). The mean of  $\Delta \log M$  is -0.11 for the 9 high redshift RQ objects in the select sample. The standard deviation of the mean for these 9 objects, if drawn from a population with similar dispersion to the PG sample, would be about 0.2 dex. For the full RQ sample, there are 23 objects with a mean  $\Delta \log M$  of -0.15, which suggests that there is no significant bias in our select sample. These results indicate that, at times corresponding to redshifts  $z \approx 2$  to 3, the average  $M_{BH}$  at a given  $\sigma_{[O III]}$  was within a factor 2 or 3 of the present day value.

One systematic uncertainty is the slope of the radius–luminosity relationship for the BLR. The high redshift RQ select objects are on average 1.8 dex more luminous than the PG sample. Use of the McLure and Jarvis (2002) relationship, with  $R \propto L^{0.61}$ , elevates the high redshift points by  $\sim 0.2$  dex in Figures 1 - 5 while having little effect on the low redshift samples. This brings the high redshift and PG samples into even closer agreement, with a mean  $\Delta \log M$  of +0.15 for the RQ PG sample and +0.14 for the RQ high redshift select sample. Figure 6 shows  $\Delta \log M$  versus redshift for the McLure and Jarvis calibration (given before equation 2 above). Another uncertainty is the slope of the  $M_{BH} - \sigma_*$  relationship, discussed by Tremaine et al. (2002). The high redshift objects in Figure 1 have  $\sigma_* \approx 500 \text{ km s}^{-1}$ . If the slope were  $M_{BH} \propto \sigma_*^{3.5}$  rather than  $\sigma_*^{4.0}$ , for example, the predicted mass for the high redshift objects would be lowered by about 0.2 dex. This would raise these objects by this amount in Figures 4 - 6.

#### 4. DISCUSSION

There are two main points that come from our analysis. First, Figures 1 and 2 show that we can place AGN on the  $M_{BH} - \sigma_*$  correlation using the [OIII] emission-line width as a surrogate for  $\sigma_*$ . This bypasses the need to obtain high signal-to-noise spectra in order to obtain the host galaxy absorption line kinematics. Nelson (2000) was the first to point this out. We confirm it with our independent data set including luminous QSOs and using photoionization masses rather than reverberation masses.

Second, given that one can measure [OIII] line profiles at fairly modest signal-to-noise levels in AGN, one can now study the relationship between black holes and their host galaxies at high redshift. Although a larger sample of high redshift objects is needed, Figures 4 - 6 suggests that the  $M_{BH} - \sigma_{[O III]}$  relationship is not a strong function of redshift. For the adopted cosmology, the age of the universe was 2.0 Gyr at  $z = 3.3$  and 3.3 Gyr at  $z = 2.0$ . The objects in this redshift range have black hole masses up to  $\sim 10^{10} M_\odot$  and implied host galaxy masses up to  $\sim 10^{13} M_\odot$ , if  $M_{\text{bulge}} \approx 10^{2.8} M_{BH}$  (Kormendy & Gebhardt 2001). Our

results suggest that black holes typically grow contemporaneously with their host galaxy bulges, or else that both were well formed by  $z \approx 3$ .

Recent results on black hole demographics suggest that high mass black holes acquire most of their mass from luminous accretion during episodes of QSO activity (Yu & Tremaine 2002, and references therein). Yu & Tremaine find that half the black hole mass is accreted before a redshift  $z \approx 1.8$ , and only 10% before  $z = 3$ . Thus, our results suggest that the black hole-galaxy bulge relationship is roughly obeyed, at least by very massive holes, at a time when much of the growth of present-day black holes lay in the future.

Previous workers have noted a tendency for [O III] widths to increase with luminosity for AGN (e.g., B96b; M99; Véron-Cetty, Véron, & Gonçalves 2001). In the present context, this is a natural consequence of the tendency to have larger  $M_{BH}$  in more luminous objects, together with the  $M_{BH} - \sigma$  relationship. B96b suggested that the mass of the host galaxy might be involved in the increase of [O III] width with luminosity.

The conclusion that galaxy growth is contemporaneous with black hole growth is consistent with chemical abundances in QSOs. Heavy element abundances in luminous QSOs are solar or several times solar (Hamann et al. 2002). The highest abundances are typically found in the centers of large galaxies (e.g., Garnett et al. 1997).

We have crudely estimated bolometric luminosities for the AGN in our sample by taking  $L_{bol} = 9\nu L_\nu(5100 \text{ \AA})$  (Kaspi et al. 2000). On average the various data sets have  $\log L_{bol}/L_{Ed} \approx -0.4$ , where the Eddington limit  $L_{Ed}$  is calculated from  $M_{BH}(H\beta)$ . This ratio shows little systematic difference between the samples at higher and lower luminosity or redshift. Some individual objects exceed the Eddington limit on this basis, but only by amounts that may be consistent with uncertainties in  $M_{BH}$  and  $L_{bol}$ .

The use of  $\sigma_{[O III]}$  provides a new way to estimate black hole masses in AGN. Once the systematics of the [O III] profile are understood in this context, black hole masses from  $\sigma_{[O III]}$  may be as reliable as “photoionization masses” based on  $H\beta$  width and continuum luminosity. The availability of two independent estimates of  $M_{BH}$  will allow workers to compare each for consistency with other approaches, such as accretion disk fitting of the continuum energy distribution (e.g., Mathur et al. 2001). Both measures of  $M_{BH}$  may likewise be examined for systematic correlations with various properties of AGN, such as the correlation of  $L/L_{Ed}$  with “eigenvector 1” found by Boroson (2002).

The  $M_{BH} - \sigma_*$  relationship offers, in principle, a new standard candle for cosmology. The value of  $M_{BH}$  derived from the broad  $H\beta$  line width varies as  $L^a$ , with  $a \approx 0.5$  to 0.6 (see discussion preceding equation 2). If one assumes that either  $\sigma_*$  or  $\sigma_{[O III]}$  correctly predicts  $M_{BH}$  through equation (1), then equation (2) can be solved for  $L$  in terms of  $\sigma_*$

and  $\text{FWHM}(\text{H}\beta)$ . This gives

$$L_{44} = 10^{0.88} \sigma_{200}^{8.02} v_{3000}^{-4}. \quad (3)$$

However, the use of equation (3) for cosmological measures will be challenging, given the large exponents of  $\sigma_{200}$  and  $v_{3000}$  and the uncertainties in the calibration of the  $M_{\text{BH}} - \sigma_{[\text{O III}]}$  and  $M_{\text{BH}} - L$  relationships.

Future work on this topic should include a systematic examination of the best way of characterizing the width of the [O III] lines for use in predicting  $\sigma_*$  and calibration of the chosen measure. Use of shorter wavelength narrow lines such as [O II] would allow study of higher redshift objects at a given observed wavelength. An obvious need is for more and better observations of the H $\beta$  and [O III] region in high redshift QSOs. In order to minimize the uncertainty associated with the scaling of BLR radius with luminosity, observations of high and low redshift QSOs should be made as nearly as possible at similar intrinsic luminosity. High resolution imaging studies may provide direct measures of the host galaxy luminosity as a check on  $\sigma_{[\text{O III}]}$ .

G.A.S. gratefully acknowledges the hospitality of Lick Observatory during summer 2001 and 2002. This material is based in part upon work supported by the Texas Advanced Research Program under Grant No. 003658-0177-2001. B.J.W. acknowledges financial support through NASA Long Term Space Astrophysics grant NAG5-3431. M.D. acknowledges support through NASA Long Term Space Astrophysics grant NAG5-3234 and NSF research grant AST99-84040. We are grateful to G. Blumenthal, T. Boroson, A. Gonçalves, D. Grupe, E. Hooper, J. Kormendy, A. Laor, J. Miller, and D. Osterbrock for helpful discussions.

## REFERENCES

- Adams, F. C., Graff, D.S., & Richstone, D. O. 2001, *ApJ*, 551, L31
- Allen, 1973, *Astrophysical Quantities* (London: Athlone Press)
- Balberg, S. & Shapiro, S. L. 2002, *Phys. Rev. Lett.*, 88, 101301 (astro-ph/0111176)
- Bernardi, M., et al. 2001, preprint (astro-ph/0110344)
- Boroson, T. A. 2002, *ApJ*, 565, 78
- Boroson, T. A., & Green, R. F. 1992, *ApJS*, 80, 109
- Brotherton, M. S. 1996a, Ph.D. Dissertation, University of Texas at Austin (B96a)

- Brotherton, M. S. 1996b, *ApJS*, 102, 1 (B96b)
- Brotherton, M. S. 2002, personal communication
- Burkert, A., & Silk, J. 2001, *ApJ*, 554, L151
- Condon, J. J., Cotton, W. D., Greisen, E. W., Yin, Q. F., Perley, R. A., Taylor, G. B., & Broderick, J. J. 1998, *AJ*, 115, 1693.
- Dietrich, M., Appenzeller, I., Vestergaard, M., & Wagner, S. J, 2002, *ApJ*, 564, 581 (D02)
- Ferrarese, L., & Merritt, D. 2000, *ApJ*, 539, L9
- Ferrarese, L., Pogge, R. W., Peterson, B. M., Merritt, D., Wandel, A., & Joseph, C. L. 2001, *ApJ*, 555, L79
- Forbes, D. A., & Ponman, T. 1999, *MNRAS*, 309, 623
- Garnett, D. R., Shields, G. A., Skillman, E. D., Sagan, S. P., & Dufour, R. J. 1997, *ApJ*, 489, 63
- Gebhardt, K., et al. 2000a, *ApJ*, 539, L13
- Gebhardt, K., et al. 2000b, *ApJ*, 543, L5
- Grupe, D. 1996, Ph. D. Thesis, Göttingen University
- Grupe, D., Beuermann, K., Mannheim, K., & Thomas, H.-C. 1999, *A&A*, 350, 805 (G99)
- Haehnelt, M. & Kauffman, G. 2000, *MNRAS*, 318, L35
- Hamann, F., Korista, K. T., Ferland, G. J., Warner, C., & Baldwin, J. 2002. *ApJ*, 564, 592
- Hooper, E. J., Impey, C. D., Foltz, C. B., & Hewett, P. C. 1995, *ApJ*, 445, 62
- Kaspi, S. et al. 2000, *ApJ*, 533, 631
- Kellermann, K. I., Sramek, R., Schmidt, M., Shaffer, D. B., & Green, R. F. 1989, *AJ*, 98, 1195
- Kellermann et al. 1994, *AJ*, 108, 1163
- Kochanek, C. 2002, personal communication
- Kormendy, J., & Gebhardt, K. 2001, in *The 20th Texas Symposium on Relativistic Astrophysics*, ed. H. Martel & J. C. Wheeler (AIP), 363

- Kormendy, J., & Richstone, D. 1995, *ARA&A*, 33, 581
- Laor, A. 1998, *ApJ*, 505, L83
- Laor., Fiore, F., Elvis, M., Wilkes, B. J. , McDowell, J. C. 1997, *ApJ*, 477, 93
- Maggorian, J. et al. 1998, *AJ*, 115, 2285
- Maoz, D. 2002, preprint (astro-ph/0207295)
- Mathur, S., Kuraszekiewicz, J., & Czerny, B. 2001, *New Astronomy*, 6, 321
- McIntosh, D. H., Rieke, M. J., Rix, H.-W., Foltz, C. B., & Weymann, R. J. 1999, *ApJ*, 514, 40 (M99)
- McLure, R. J. & Dunlop, J. S. 2001, *MNRAS*, 327, 199
- McLure, R. J., & Jarvis, M. J. 2002, *MNRAS*, in press (astro-ph/0204473)
- Michalitsianos, A. G., Falco, E. E., Munoz, J. A., & Kazanas, D. 1997, *ApJ*, 487, L117
- Morris, S. L., Weymann, R. J., Anderson, S. F., Hewett, P. C., Foltz, C. B., Chaffee, F. H., Francis, P. J., and MacAlpine, G. M. 1991, *AJ*, 102, 1627
- Nelson, C. H. 2000, *ApJ*, 544, L91
- Nelson, C. H., & Whittle, M. 1995, *ApJS*, 99, 67
- Nelson, C. H., & Whittle, M. 1996, *ApJ*, 465, 96
- Netzer, H. et al. 1995, *ApJ*, 448, 27
- Neugebauer, G., Green, R. F., Matthews, K., Schmidt, M., Soifer, B. T., & Bennett, J. 1987, *ApJS*, 63, 615
- Netzer, H., & Laor, A. 1993, *ApJ*, 404, L51
- Ostriker, J. 2001, *Phys. Rev. Lett.* 84, 5258
- Peterson, B. 1993, *PASP*, 105, 247
- Peterson, B. 1997, *An Introduction to Active Galactic Nuclei*, (Cambridge: Cambridge University Press).
- Richstone, D. et al. 1999, *Nature*, 395, A14



- Schmidt, M., & Green, R. F. 1983, *ApJ*, 269, 352
- Silk, J., & Rees, M. J. 1998, *A&A*, 331, L1
- Tremaine, S., et al. 2002, *ApJ*, 574, 740
- Véron-Cetty, M.-P. & Véron, P. 1989, *A Catalog of Quasars and Active Galactic Nuclei* (ESO Sci. Rep. 7)(4th ed.; Garching: ESO)
- Véron-Cetty, M.-P., Véron, P., & Gonçalves, A. 2001, *A&A*, 327, 730
- Vestergaard, M. 2002, *ApJ*, 571, 733
- Wandel, A., Peterson, B. M., & Malkan, M. A. 1999 *ApJ*, 526, 579
- Wandel, A. 2001, *ApJ*, 565, 762
- Wills, B. J. et al. 1995, *ApJ*, 447, 139
- Wills, B. J., & Brotherton, M. S. 2002, person communication
- Wilson, A. S., & Heckman, T. M. 1985, in *Astrophysics of Active Galaxies and Quasi-stellar Objects*, Ed. J. S. Miller (Mill Valley, CA: University Science Books)
- Yu, Q. & Tremaine, S. 2002, *MNRAS*, 335, 965

Table 1. [OIII] Widths of PG Quasars

Name PG	Date UT 1996	Integration seconds	EW(FeII) Å	Fe II/H $\beta$	FWHM([OIII]) km s $^{-1}$
0947+396	Feb 14	2700	25	0.22	366 $\pm$ 13
0953+414	Feb 15	2100	39	0.30	571 19
1001+054	Feb 15	2700	73	0.74	678 7
1048+342	Feb 14	2700	73	0.57	286 9
1114+445	Feb 15	2400	20	0.19	538 8
1115+407	Feb 15	2700	33	0.42	224 17
1115+407	Feb 16	2700	...	...	267 24
1116+215	Feb 15	2400	81	0.43	902 7
1116+215	Feb 16	2700	...	...	901 18
1202+281	Feb 14	2100	20	0.12	412 8
1216+069	Feb 17	2400	8	0.04	343 16
1226+023	Feb 17	600	6	0.05	754 20
1309+355	Feb 14	2400	14	0.22	641 12
1322+659	Feb 14	2700	45	0.66	249 15
1352+183	Feb 14	2400	61	0.51	572 8
1411+442	Feb 15	2400	52	0.49	411 10
1427+480	Feb 16	2400	50	0.35	476 28
1440+356	Feb 15	1800	76	1.15	464 8
1626+554	Feb 14	2201	46	0.31	694 23

Note. — Equivalent width, EW(FeII), is measured in the rest frame using the Boroson & Green (1992) FeII template. The full width at half the maximum of the line profile, FWHM, is determined by direct measurement from the FeII-corrected [O III] profile, not from an analytical fit. Values have been corrected by subtracting the instrumental FWHM in quadrature. Uncertainties are estimated rms, including uncertainties from noise and in correcting for instrumental resolution, but not including uncertainties in FeII subtraction. The Fe II measurements refer to the region between 4434Å and 4686Å in the original I Zw 1 template constructed by Boroson & Green (1992), that is, they refer to a template with I Zw 1’s line profile.

Table 2.  $M_{BH}$  and  $\sigma_{[O III]}$  for AGN

Name	Alternate Name	RL/RQ	z	FWHM(H $\beta$ ) km/s	log( $\nu L_\nu$ ) erg/s	log(M <sub>BH</sub> ) M <sub>☉</sub>	log( $\sigma_{[O III]}$ ) km/s
<i>D02</i>							
0256-0000		L	3.377	4455	46.85	9.46	2.55
0302-0019		Q	3.286	3777	46.89	9.33	2.50
<i>M99</i>							
0153+744		L	2.341	5650	47.16	9.82	2.70
0421+019		L	2.056	4660	46.63	9.39	2.77
0424-131		L	2.168	4380	46.50	9.27	2.70
1331+170		L	2.097	7480	46.98	9.97	2.88
0043+008		Q	2.146	4330	46.69	9.35	2.59
0109+022		Q	2.351	7020	46.68	9.77	2.77
1104-181		Q	2.318	3950	47.07	9.46	2.78
2212-179		Q	2.228	6150	46.76	9.69	2.71
<i>B96a</i>							
0024+22	NAB	L	1.109	5883	46.34	9.45	2.70
0424-13	PKS	L	2.167	4818	46.60	9.40	2.78
0454+03	PKS	L	1.345	4896	46.54	9.39	2.46
0952+179	PKS	L	1.476	4574	46.35	9.23	2.52
1718+48	PG	L	1.082	4613	47.06	9.59	2.83
0117+213	PG	Q	1.499	6493	46.84	9.78	2.77
0920+580	SBS	Q	1.378	4928	46.18	9.21	2.47
1120+01	UM 425	Q	1.470	6821	46.64	9.72	2.75
1634+706	PG	Q	1.335	9601	47.21	10.30	2.94
<i>B96b</i>							
0159-117	3C 057	L	0.670	4500	45.76	8.92	2.42
0414-060	3C 110	L	0.773	8200	45.91	9.52	2.39
0736+017	0	L	0.191	3400	44.74	8.17	2.36
0738+313	0	L	0.630	4800	45.60	8.90	2.19
0742+318	0	L	0.462	9940	45.74	9.60	2.29
0838+133	0	L	0.684	3000	45.40	8.39	2.19

Table 2—Continued

Name	Alternate Name	RL/RQ	$z$	FWHM(H $\beta$ ) km/s	$\log(\nu L_\nu)$ erg/s	$\log(M_{\text{BH}})$ $M_\odot$	$\log(\sigma_{\text{OIII}})$ km/s
0903+169	3C 215	L	0.411	4440	44.63	8.35	2.34
0923+392	0	L	0.698	7200	45.84	9.37	2.34
1004+130	PG	L	0.240	6300	45.22	8.94	2.30
1007+417	0	L	0.613	3560	45.61	8.65	2.34
1011+232	0	L	0.565	2700	45.23	8.21	2.17
1100+772	PG	L	0.311	6160	45.40	9.01	2.41
1103-006	PG	L	0.426	6560	45.26	9.00	2.52
1137+660	3C 263	L	0.652	6060	46.03	9.32	2.38
1150+497	0	L	0.334	4810	44.85	8.52	2.22
1217+023	0	L	0.240	4300	45.12	8.56	2.21
1250+568	SBS	L	0.320	4560	44.53	8.32	2.33
1305+069	3C 281	L	0.599	6440	45.28	9.00	2.46
1340+290	0	L	0.905	13000	45.83	9.88	2.28
1354+195	0	L	0.720	4400	45.95	9.00	2.30
1458+718	0	L	0.905	3000	45.64	8.51	2.46
1545+210	0	L	0.264	7030	45.04	8.95	2.33
1750+175	0	L	0.507	3700	45.45	8.60	2.34
<i>PG</i>							
1226+023	3C 273	L	0.158	3520	46.10	8.88	2.51
1309+355	Ton 1565	L	0.182	2940	44.98	8.16	2.44
0947+396	K347-45	Q	0.206	4830	44.88	8.54	2.19
0953+414	K348-7	Q	0.234	3130	45.56	8.51	2.39
1001+054		Q	0.161	1740	44.87	7.65	2.46
1048+342		Q	0.167	3600	44.80	8.25	2.09
1114+445		Q	0.144	4570	44.73	8.42	2.36
1116+215	TON 1388	Q	0.176	2920	45.54	8.44	2.58
1202+281	GQ Com	Q	0.166	5050	44.66	8.47	2.24
1216+069		Q	0.332	5190	45.65	8.99	2.16
1322+659		Q	0.168	2790	44.92	8.09	2.03
1352+183	PB 4142	Q	0.151	3600	44.91	8.30	2.39
1411+442	PB1732	Q	0.090	2670	44.56	7.87	2.24

Table 2—Continued

Name	Alternate Name	RL/RQ	$z$	FWHM( $H\beta$ ) km/s	$\log(\nu L_\nu)$ erg/s	$\log(M_{\text{BH}})$ $M_\odot$	$\log(\sigma_{\text{OIII}})$ km/s
1427+480		Q	0.220	2540	44.89	7.99	2.31
1440+356	Mrk 478	Q	0.077	1450	44.53	7.33	2.30
1626+554		Q	0.132	4490	44.66	8.37	2.47
<i>G99</i>							
RX J0022-34		Q	0.219	4110	44.97	8.45	2.18
ESO 242-G8		Q	0.059	3670	43.77	7.75	2.12
RX J0100-51		Q	0.062	3450	44.10	7.86	2.38
RX J0152-23		Q	0.113	3510	44.56	8.10	2.46
RX J0204-51		Q	0.151	5990	44.42	8.50	2.12
RX J0319-26		Q	0.079	4170	44.11	8.03	2.31
RX J0323-49		Q	0.071	2075	43.78	7.26	1.99
ESO 301-G13		Q	0.064	3180	44.08	7.78	2.37
VCV 0331-37		Q	0.064	2165	43.76	7.29	1.86
Fairall 1116		Q	0.059	4560	44.13	8.12	2.13
RX J0425-57		Q	0.104	2900	45.08	8.20	2.28
Fairall 303		Q	0.040	1720	43.39	6.90	1.78
RX J0435-46		Q	0.070	3820	43.52	7.66	2.04
RX J0437-47		Q	0.052	4215	43.98	7.98	2.01
RX J0438-61		Q	0.069	2410	44.07	7.54	1.91
CBS 126		Q	0.079	2850	44.31	7.80	2.20
Mkn 141		Q	0.042	4175	43.87	7.91	2.23
Mkn 734		Q	0.033	2230	43.94	7.40	2.28
IRAS 1239+33		Q	0.044	1900	43.91	7.25	2.31
RX J1646+39		Q	0.100	2160	43.85	7.33	1.99
RX J2232-41		Q	0.075	4490	43.67	7.87	2.29
RX J2245-46		Q	0.201	2760	45.41	8.32	2.46
RX J2248-51		Q	0.102	3460	44.50	8.07	1.99
MS 2254-37		Q	0.039	1545	43.84	7.04	2.41
RX J2258-26		Q	0.076	2815	44.00	7.63	2.08
RX J2349-31		Q	0.135	5210	44.32	8.33	2.31

Note. — Black hole mass and [O III] line width for AGN as described in the text. Columns give (1) reference (*italicized*) or object name, (2) other name, (3) radio loud (L) or quiet (Q), (4) redshift, (5) FWHM of the broad  $H\beta$  line, (6) continuum luminosity ( $\nu L_\nu$ ) at 5100 Å rest wavelength, (7) black hole mass from equation (2), and (8)  $\sigma_{[\text{O III}]}$   $\equiv$  FWHM([O III])/2.35. References are D02: Dietrich et al. (2002), M99: McIntosh et al. (1999), B96a: Brotherton (1996a), B96b: Brotherton (1996b), PG: this paper, G99: Grupe et al. (1999). See text for discussion of continuum measurements.

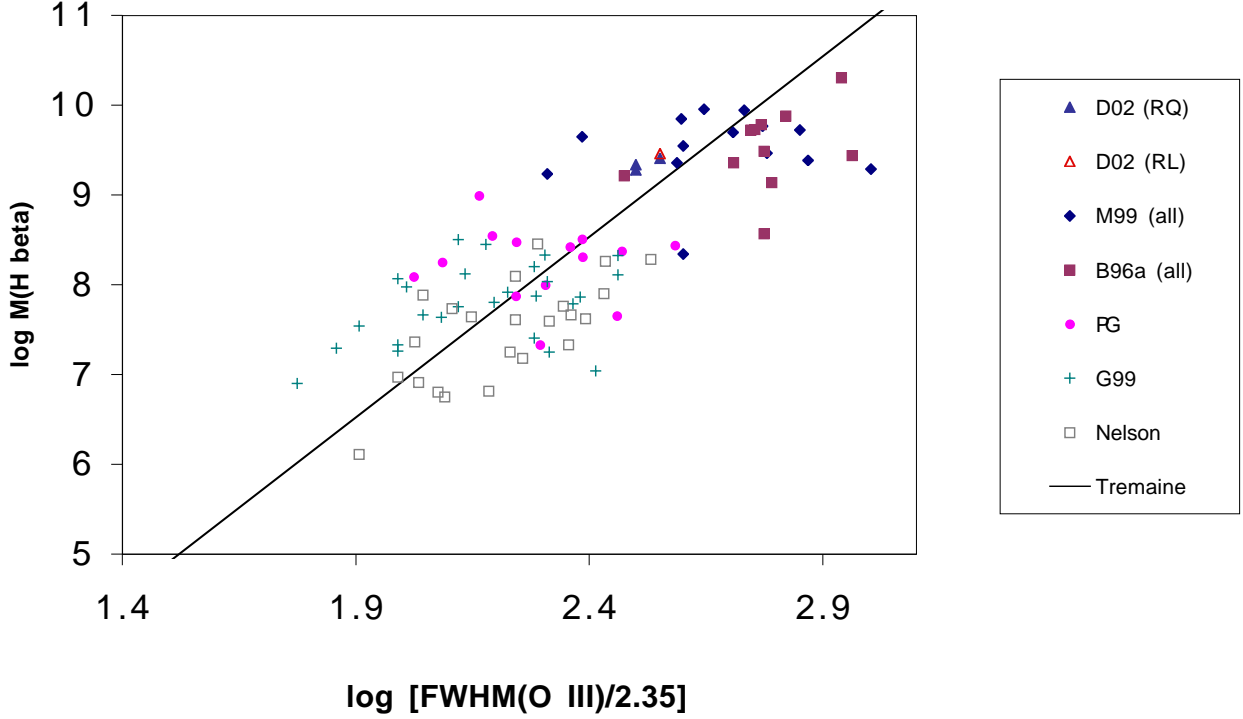


Fig. 1.— Black hole mass derived from  $\text{H}\beta$  line width and continuum luminosity versus width of the  $[\text{O III}]$  line for radio quiet AGN (see text). Line is the  $M_{BH} - \sigma_*$  relation from Tremaine et al. (2002), given by equation (1); it is not a fit to the QSO data. Shown here are the “full” data sets from M99 and B96a, which include some highly uncertain values (see text). Key to data sources is given in the footnote to Table 2: triangles—D02; diamonds—M99; squares—B96a; dots—FG; crosses—G99. Because of the scarcity of high redshift points, we include as an open triangle the D02 object Q0256-0000, which barely exceeds the threshold to be classified radio loud.

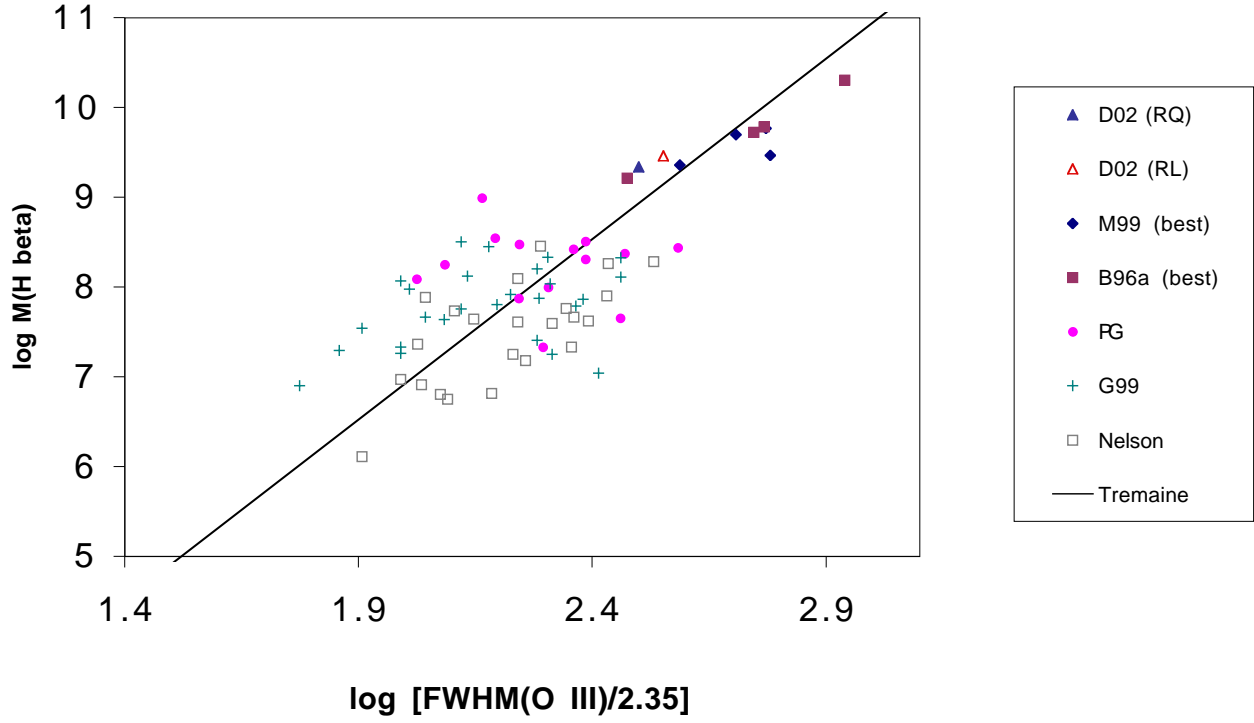


Fig. 2.— Same as Figure 2 but for the “select” data sets from M99 and B96a. See text for discussion of errors.

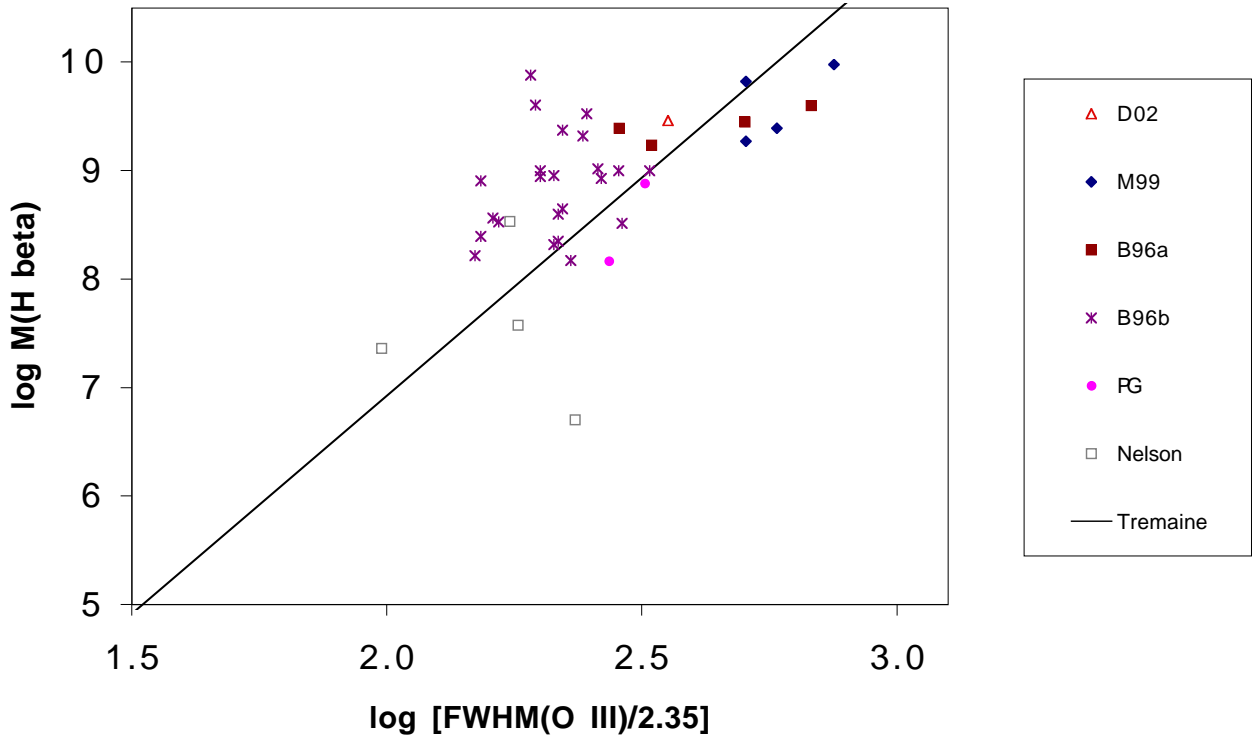


Fig. 3.— Same as Figure 2 but for radio loud AGN. B96b data are shown as asterisks.



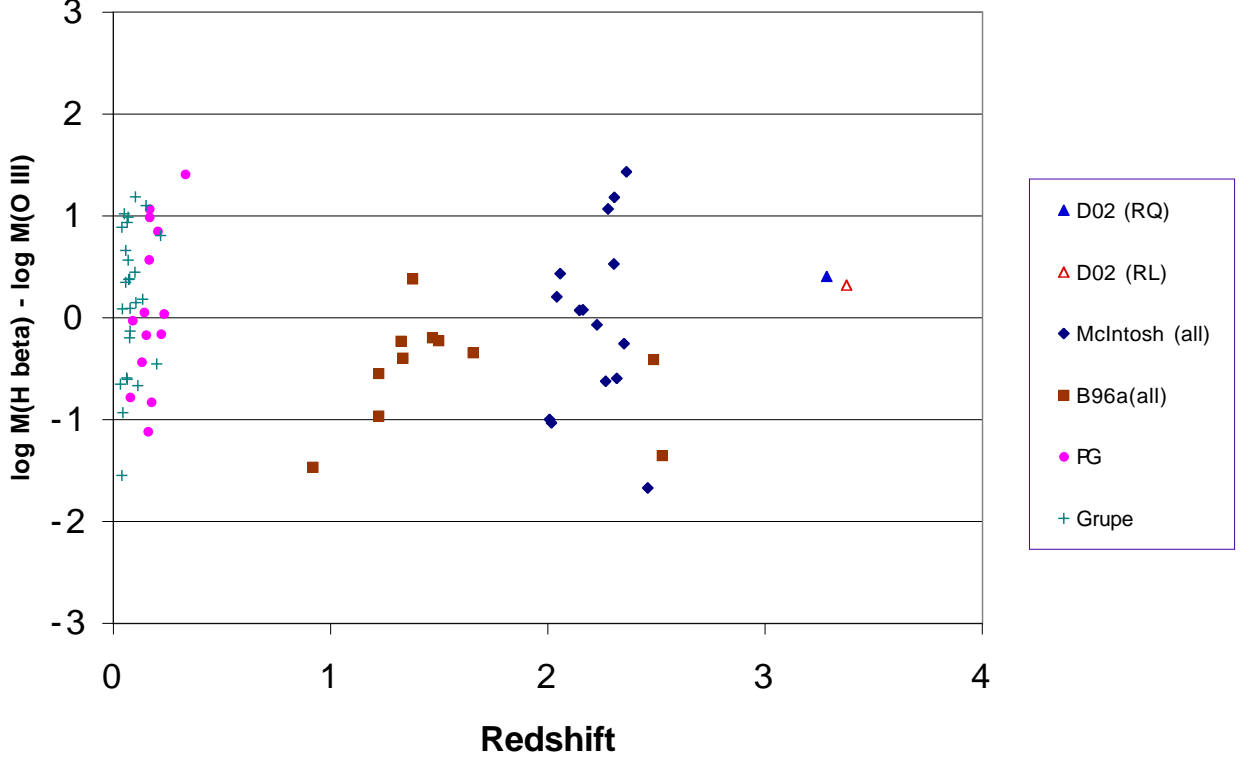


Fig. 4.— Redshift dependence of the departure of measured black hole mass from value expected from the  $M_{BH} - \sigma_*$  relationship (equation 1) and the measured [O III] line width for radio quiet AGN (see text). Ordinate is  $\Delta \log M \equiv \log M_{BH} - \log M_{[O III]}$ , where  $M_{BH}$  is the black hole mass derived from the  $H\beta$  line width and continuum luminosity (equation 2) and  $M_{[O III]}$  is the black hole mass expected from the measured [O III] line width on the basis of equation (1). Shown here are the “full” data sets from M99 and B96a. The high redshift QSOs do not differ significantly in the mean from the low redshift objects in the relationship between black hole mass and [O III] line width. This indicates little or no change in the  $M_{BH} - \sigma_*$  relation since the universe was 2 to 3 billion years old.

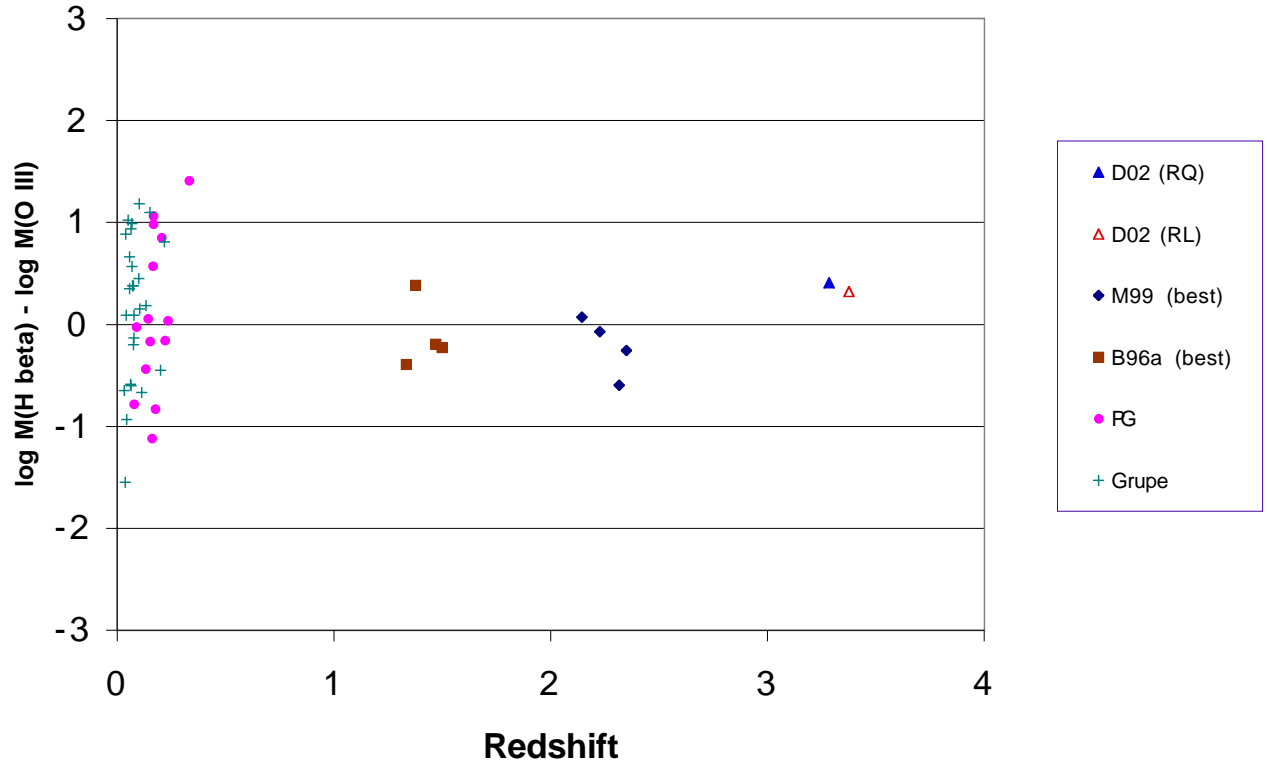


Fig. 5.— Same as Figure 4 but for the “select” data sets from M99 and B96a.

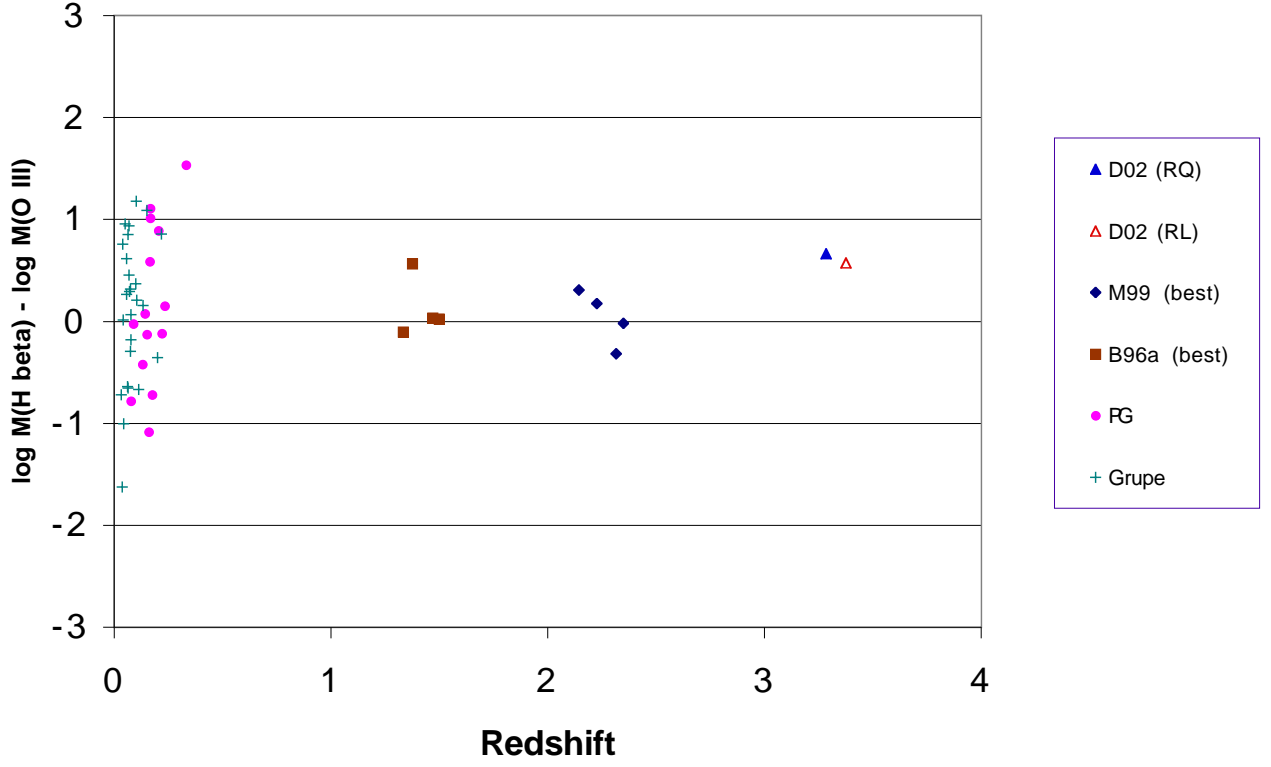


Fig. 6.— Same as Figure 5 but for  $M_{BH} = (10^{7.63} M_{\odot})v_{3000}^2 L_{44}^{0.61}$  (see text).